KSME

Springer

Journal of Mechanical Science and Technology 36 (8) 2022

Original Article
DOI 10.1007/s12206-022-0747-9

Keywords:
· Fibrous materials
· Porous sound absorber
· Ethanol flame
· Thermoacoustic oscillation

Correspondence to:
Hao Zhou
zhouhao@zju.edu.cn

Citation:
Zhou, H., Fang, H., Wei, D., Liu, Z., Wang, Z., Meng, H. (2022). Control of thermoacoustic instability of liquid-spray flame with porous sound absorber. Journal of Mechanical Science and Technology 36 (8) (2022) 4303~4313.
http://doi.org/10.1007/s12206-022-0747-9

Received December 30th, 2021
Revised February 28th, 2022
Accepted April 6th, 2022

† Recommended by Editor
Tong Seop Kim

Control of thermoacoustic instability of liquid-spray flame with porous sound absorber

Hao Zhou, Hao Fang, Dongliang Wei, Zihua Liu, Zhaowen Wang and Hanxiao Meng

State Key Laboratory of Clean Energy Utilization, Zhejiang University, Zheda Road 38, Hangzhou 310027, China

Abstract A kind of porous sound absorber was studied to control the thermoacoustic oscillation of liquid mist flame, which combined natural fibrous materials and perforated plate. It could optimize the sound absorption characteristics of fibrous materials by adding perforated plate and air cavity. The influences of the interlayer and back cavity depth of two kinds of fibrous materials with the mass of 20, 30, 40 g were investigated experimentally in an impedance tube and applied to control the oscillating ethanol flame. The results showed that the best depth of interlayer and back cavity were 20 cm and 30 cm, respectively. The addition of two kinds of fiber sandwich structures could reduce the amplitude of the sound pressure oscillation in the combustion chamber by 89.2 % and 92.6 %, as well as 88.0 % and 91.2 % in the plenum chamber, meanwhile, restrained the flame heat release fluctuation by 73 %. It was proved that the porous sound absorber could act as a damp in the acoustic transmission path and suppress the sound source.

1. Introduction

To meet the strict requirements of NOx emission, modern gas turbines widely adopt lean premixed combustion. It can effectively reduce the temperature peak of the flame and reduce the generation of NOx. Unfortunately, it also frequently gives rise to the occurrence of "thermoacoustic instability" [1-4], which is a common phenomenon encountered by modern low NOx gas turbines [5]. Thermoacoustic instability is reflected explicitly in the pressure pulsation and intense noise in the burner. It is a combustion instability phenomenon caused by the coupling between the heat release pulsation of flame and the inherent acoustic pulse of the combustor in the combustion process, the essential condition of which is the Rayleigh criterion [6-9]. Compared with gas premixed combustion, the instability of swirling liquid combustion is more complicated to understand. The atomization and vaporization process of fuel droplets, the spatial distribution of droplets in the combustion area, as well as the interaction between spray and vortex of flame, will affect the heat release process [10-12].

As a sound-absorbing material, natural fibrous materials have the excellent characteristics of low densities, good mechanical properties, easy processing, and low cost [13, 14]. With public attention to the ecological environment and the exploration of natural resources, the utilization of renewable materials has gradually attracted the attention of scholars [15, 16]. They are considered to be used to control the oscillating sound wave generated by combustion instability. When the sound wave enters the material, the air in the hole chamber rubs and vibrates with the hole wall to produce viscous resistance, so as to dissipate the sound energy, eventually achieving the sound absorption. Simultaneously, due to the temperature gradient in the materials, the sound energy can be transformed into thermal energy by heat conduction. Moreover, the fibrous materials themselves have a particular natural frequency and will resonate under the sound of a specific frequency, which also plays a role in sound energy attenuation.

Natural fibrous materials have excellent sound absorption characteristics. Berardi [17] meas-

ured the sound absorption coefficient and airflow resistance of kenaf, wood, hemp, coconut, cork, sugarcane, paperboard, and wool fibers, confirming the feasibility of natural fibrous materials as an acoustic absorption damper. Sample thickness [18-22], porosity [22, 23], and fiber diameter [22-24] are essential factors affecting the sound absorption coefficient, which have been widely studied by researchers [25]. Three kinds of samples of 60 mm, 80 mm, and 120 mm with broom fiber were prepared, and they proved that with the increase of the sample thicknesses, the peak value of the sound absorption coefficient gradually moved to the low-frequency band [19]. Bakri [18] pointed out a positive correlation between the sound absorption coefficient and the sample thickness in the low and medium frequency range. However, in the high-frequency band of 4000-6000 Hz, the sound absorption coefficient began to decrease gradually when the sample thickness exceeded 20 mm. Lignin adsorption exists on the surface of natural fibrous materials [26], which will affect the sound absorption process. Chemical soaking is a mainstream treatment method at present, especially alkali solution. Sodium hydroxide (NaOH)/alkali treatment proved its ability to improve microstructure by changing the chemical composition of towel gourd fiber and removing all impurities [27-30]. Nasidi [31] employed NaOH with a concentration in a range of 1 %-8 % to process the surface of coconut fiber. It was concluded that with the increase of NaOH concentration, the diameter of fibrous material decreased with scanning electron microscope (SEM). Acoustic tested showed that the average sound absorption coefficient in a low and high-frequency band was more than 0.9 after treatment with 7 % and 8 % NaOH, which greatly enhanced the sound absorption capacity. Cao [32] summarized that compared with perforated panels and membrane resonators, porous materials have the advantages of high sound absorption frequency and low cost, but the thickness and structure of materials still need to be further optimized to enhance practical application.

In order to better predict the sound absorption effect of materials, scholars put forward numerous empirical models based on experiments. The only parameter of airflow resistance was required to predict the acoustic characteristics with the Delany-Bazley model, proposed in 1969 [33]. Bhingare [20] calculated the influence of sample thickness and density on sound absorption coefficient with the model, and pointed out that the greater the sample density is, the better the sound absorption effect is under the same thickness. David [34] applied Delany-Bazely model and Garai-Pompoli model to predict the sound absorption of natural fiber, and compared it with the experimental results. It was found that the overall trend of sound absorption prediction of jute material was similar to the measurement, but the consistency was not good. Nevertheless, for the reason that the Delany-Bazley model was established based on the range of 1-10 μm, there are limitations in applying larger diameter fibrous materials. Garai and Pompoli [35] conducted experiments with diameters of about 20-50 μm polyester fiber to further modify the Delany-Bazley model coefficient, which is more adaptable in large-diameter natural fibrous materials. But the best suitable method is limited to a specific frequency range. Allard and Champoux [36] proposed a simplified approach to minimize the Delany-Bazley model error at low frequencies with high curvature and porosity. In the new formula, dynamic density $\rho(\omega)$ is related to the inertial force and viscous force per unit air volume when sound waves pass through the absorbing material.

The limited sound absorption capacity of single fibrous material in low frequency limits its application and development. To broaden the scope of use, its structural modification is an effective method. Ayub [37] designed a double-layer fiber structure and discussed the influence of air chambers on sound absorption performance. Putra et al. [21] found that increasing the depth of the air back cavity in the low-frequency band is conducive to improving the sound absorption coefficient.

At present, most of the researches focused on the sound absorption of single fibrous materials. Few people studied the sound absorption characteristics of the sound absorber composed of porous fibrous material and perforated plate, let alone the practical thermal application. Due to the acoustic oscillation mainly occurring at low frequency, the combined sound-absorbing structure with air interlayer and back cavity was composed of fibrous material and perforated plate for low frequency sound absorption control in our study. We measured the flow resistance of porous fiber materials (Sec. 3.1). And the sound absorption characteristics of low intermediate frequency, the effects of interlayer depth and back cavity depth on sound absorption were evaluated (Sec. 3.2-3.4). In addition, the structure was applied to the liquid-spray flame self-excited rig to control the combustion oscillation of ethanol flame (Sec. 3.5).

2. Experimental setup

2.1 Materials

Coconut fiber is mainly produced in Southeast Asian countries such as Thailand, Vietnam and India. It is also mass-produced in Hainan province in China due to its geographical location in the tropics. Palm trees are mainly distributed in the south and southwest of Guangxi and Yunnan Province in China.

Coconut fiber and palm bark fiber were selected as natural fibrous materials, 20 g, 30 g and 40 g of which were weighed by electronic balance. The self-made mold with an inner diameter of 100 mm (as shown in Fig. 1(b)) was applied to press the samples on the tablet press (YP-15T, Tianjin, China, as shown in Fig. 1(a)). The pressing pressure was 20 MPa and maintained under the pressing pressure for 5 min. After that, they were put in the atmosphere environment to expand freely for 48 h to obtain each sample, as shown in Fig. 1(c). We made use of a vernier caliper to measure the thicknesses of each samples after full expansion and number them, as shown in Table 1. On account of the hard palm bark fiber, the greater the quality was, the greater the difficulty of compression became. Therefore, the thickness of Z40 was 4 mm thicker than Y40.

Table 1. Main properties of the materials studied in this paper.

Numbers of samples	Materials	Mass m_0 (g)	Thickness l (mm)	Density ρ (kg/m^3)
Y20	Coconut fiber	20	28	90.95
Y30	Coconut fiber	30	44	86.91
Y40	Coconut fiber	40	56	90.95
Z20	Palm bark fiber	20	28	90.95
Z30	Palm bark fiber	30	44	86.91
Z40	Palm bark fiber	40	60	84.88

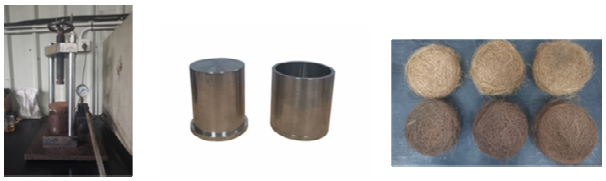

(a) (b) (c)

Fig. 1. Sample preparation of fibrous materials: (a) table machine; (b) sample mould; (c) fiber samples.

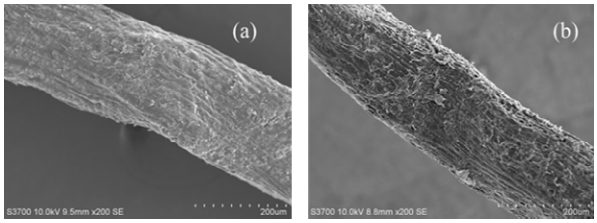

Fig. 2. The microscopic images of (a) coconut fiber; (b) palm bark fiber by SEM.

In order to compare the microstructure of coconut fiber and palm bark fiber, the samples were photographed by tungsten filament SEM (Hitachi, S-3700N), with a maximum resolution of $\leq$0.8 nm. The captured image is shown in Fig. 2, and the magnification is ×200. The surface of the two kinds of fibrous materials were covered by impurities, and the surface is not flat, including pectin, wax, lignin and silica. The uneven structure forms small intervals, which provides favorable conditions for sound absorption. On the basis of the given measuring scale, the average fiber diameter of coconut fiber can be calculated as 229 μm and palm bark fiber 210 μm. After pressing, two kinds of fibers are staggered with each other to form porous structure airflow passes through.

The perforated plate used in this study was made of brass, and the parameter characteristics are shown in Table 2 and Fig. 3(a). As for the control of perforated plate on incident sound wave and flame combustion instability, our previous study Ref. [38] has already been introduced.

2.2 Acoustic measurement

It can be seen from Fig. 4, the length of the impedance tube is 1015 mm, and the inner diameter is 100 mm, whose tested

Table 2. Parameters of perforated plate studied in this paper.

Parameters	a (mm)	d (mm)	σ (%)	h (mm)
Values	1.00	10.00	3.14	1.00

Note: a is the aperture radius, d is the orifice spacing, σ is the porosity, h is the specimen thickness.

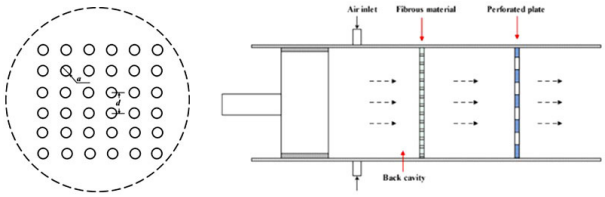

Fig. 3. The schematic diagram of (a) the perforated plate; (b) the back cavity.

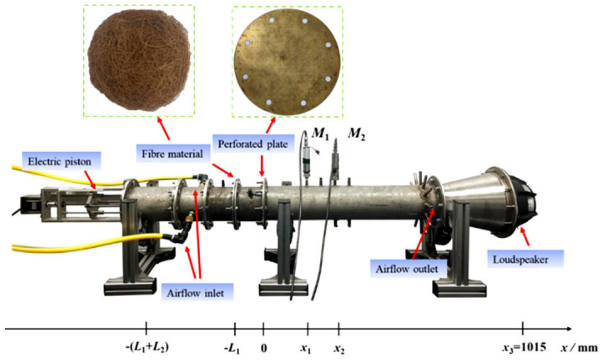

Fig. 4. The acoustic impedance measurement system with fibrous material and perforated plate.

frequency range is from 100 Hz-1600 Hz. And the corresponding Helmholtz number range is below 0.463 [39]. The left end of the acoustic impedance tube was an adjustable back cavity with an electric piston. The piston location could be adjusted by the controller, whose adjustment range was 0-150 mm and the accuracy were 0.35 mm. Normal temperature and pressure air (300 K, 101.3 kPa) was delivered from airflow inlet to the chamber through the float flowmeter supplied by a forced draft fan. The range of the float flowmeter was 0-10 m^3/h and the accuracy were 0.5 m^3/h. The perforated plate was installed at x = 0. And the right side of the fibrous material with a certain thickness was at x = -L_1. The forced frequency and amplitude of the incident sound wave were independently controlled by the signal generator (GWINSTEK, Taipei, China, AFG-2105), whose range was 0.1~5 MHz and the accuracy were 0.1 Hz. Then the signal was amplified by the connected power amplifier (YAMAHA, P 50000S) and output to the loudspeaker assembled at x_3 = 1015 mm. In this research, the sound pressure level (SPL) of the loudspeaker was fixed at 105 dB. Two dynamic pressure sensors M_1 and M_2 (CYG type 1406, Suzhou, China) was inserted on the impedance pipe to measure the

sound pressure pulsation in the impedance pipe. The sensors has been statically calibrated with calibration gas N_2 on a standard sound pressure test bench (pressure range: 0-35 kPa, accuracy: ±0.05 % FS), and NI-MAX was used for self-calibration before the test. For acoustic wave measurement in different frequency bands, the distance between the two sensors was determined according to ISO 10534-2-1998 [40]. When the incident sound frequency f > 340 Hz, the distance between the two sensors was s = 10 cm, and when f < 340 Hz, s = 5 cm. The NI acquisition card (USB-6210) and software LabVIEW were adapted for data collection and analysis, sampling rate and time of which were 20 kHz and 5 s.

Based on the double microphone transfer function and sensor switching technology, the specific acoustic impedance is calculated by

$$\zeta(\omega) = j\left[\frac{H_{12}\sin(\omega x_1 / c_0) - \sin(\omega x_2 / c_0)}{\cos(\omega x_2 / c_0) - H_{12}\cos(\omega x_1 / c_0)}\right] \tag{1}$$

where H_{12} is the transfer function calculated from the self-spectral density and cross-spectral density of sound pressure, $\omega = 2\pi f$ is the angular frequency and $j = \sqrt{-1}$ is the imaginary unit, c_0 represents the local sound velocity, x_1 and x_2 represent the shortest distance between the dynamic pressure sensor M_1, M_2 and the perforated plate.

When the acoustic reflection coefficient of the sandwich structure is determined, the reflection coefficient R_c is determined by

$$R_c = \frac{\zeta + 1}{\zeta - 1} = |R_c| e^{j\theta}. \tag{2}$$

In the formula, $|R_c|$ and θ represent the modulus and phase of sound reflection coefficient, respectively, and the sound absorption coefficient α can be obtained from

$$\alpha = 1 - |R_c|^2. \tag{3}$$

2.3 Combustion facility

The liquid-spray flame self-excited rig is shown in Fig. 5. The thermal power of the burner was 3.5 kW and the global equivalence ratio Φ = 0.36. The square outlet section (110×110 mm) on top of the burner connected with the atmosphere, and the smoke produced by combustion is directly discharged into the environment. The burner was equipped with an air atomizer nozzle (Delavan, SNA type-30609-2). The air compressor provided 0.2 MPa atomizing air to atomize and inject ethanol fuel (C_2H_5OH, purity: 99.7 %) with a siphon height of 0.1-0.2 m into the combustion chamber. According to the nozzle characteristics, when the siphon height was at the value and the atomized air was controlled at 10 NL/min by an Alicat mass flowmeter, the ethanol atomization flow was

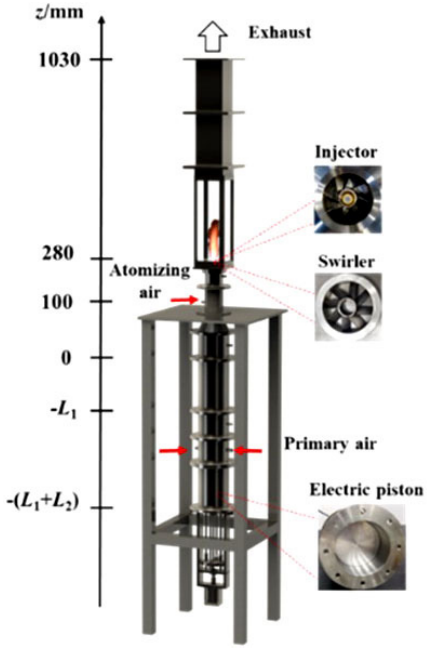

Fig. 5. Photograph of liquid spray self-excited burner equipped with injector, swirler and electric piston.

10 mL/min. The front and rear sides of the burner were quartz windows, which could provide optical observation. The swirler was axially installed directly below the nozzle, made of stainless steel, with 8 central blades with an inclination of 60° and the thickness of vanes was 1 mm. And in this work, the swirl number was S_w = 1.27 approximately calculated by the following formula due to small thickness [41]:

$$S_w = \frac{\int_{d_i/2}^{d_o/2} u_a u_\theta r^2 \mathrm{d}r}{(d_o/2)\int_{d_i/2}^{d_o/2} u_a^2 r \mathrm{d}r} \approx \frac{2}{3}\left[\frac{1-(d_i/d_o)^3}{1-(d_i/d_o)^2}\right]\tan\gamma \tag{4}$$

where d_o, d_i and γ represent swirling diameter, swirler diameter and swirl angle, u_a and u_θ were axial and tangential velocity. The primary air under normal temperature and pressure flowed through the float flowmeter from both sides of the inlet end at the bottom of the burner with a forced draft fan, and was delivered into the plenum chamber at the top of the inlet section. The perforated plate and the upper side of fibrous material were located at z = 0 and z = -L_1. The adjustable electric piston was used to adjust the depth L_2 between the lower side of the fibrous material and the rigid wall. The dynamic pressure sensor was inserted at the wall interface of the combustion and plenum chamber to test pressure fluctuation P_1 and P_2. Photomultiplier tube PMT (Hamamatsu H10722 series; cathode luminous sensitivity: 105 μA/lm; anode luminous sensitivity: 2.1×10^8 V/lm) was equipped to acquire flame CH* signal, as a measure of the global heat release fluctuation. The PMT was placed 20 cm in front of the quartz glass main window of the burner and remains stationary.

Table 3. Differential pressure before and after samples and airflow resistivity.

Samples	Differential pressure Δ*p* (Pa)	Airflow resistivity r_0 (Pa·s/m^2)
Y20	2.59	275.3
Y30	6.57	444.4
Y40	11.53	612.8
Z20	3.24	344.4
Z30	6.66	450.5
Z40	17.01	843.7

3. Results and discussion

3.1 Airflow resistance measurement of fibrous materials

Airflow resistance is the resistance of air flowing through fibrous materials measured by airflow resistivity. The greater airflow resistivity stands for the flow difficulty. In comparison, small airflow resistivity is generally considered to be the larger pores formed between fibers. It is reported that the airflow resistivity is inversely proportional to the square of pore size, and the airflow can pass smoothly with less interference [42]. Flow resistance can be obtained from [43, 44]

$$R = \frac{\Delta p}{q_v} \tag{5}$$

$$r_0 = \frac{R \cdot A}{l} \tag{6}$$

where R is the flow resistance of the material, Pa·s/m^3; Δp is the differential pressure before and after the sample, Pa; q_v is the airflow in the pipeline, m^3/s; r_0 is the flow resistivity of the material, Pa·s/m^2; l is the thickness of the sample, m; A is the cross-sectional area of the fibrous material perpendicular to the airflow direction, m^2.

3.2 Airflow resistance measurement of fibrous materials

Most of the sound absorption models of fiber materials are empirical formulas, which are based on the Delan-Bazley model [33], and only the flow resistivity is used to predict the sound absorption characteristics.

$$z_c = \rho_0 c_0 \left\{1 + c_1\left(\frac{\rho_0 f}{r_0}\right)^{c_2} + j\left[c_3\left(\frac{\rho_0 f}{r_0}\right)^{c_4}\right]\right\} \tag{7}$$

$$k_c = \frac{\omega}{c}\left\{1 + c_5\left(\frac{\rho_0 f}{r_0}\right)^{c_6} - j\left[c_7\left(\frac{\rho_0 f}{r_0}\right)^{c_8}\right]\right\} \tag{8}$$

where z_c is the characteristic impedance; k_c is the complex wave number of the fibrous materials; ρ_0 is the air density; c_0 is the sound velocity; f is the frequency; r_0 is the flow resistivity; c_1-c_8 are the Delany-Bazley empirical constants.

Table 4. Empirical constants of different models.

Models	Delany-bazley	Garai-pompoli
c_1	0.0571	0.078
c_2	-0.754	-0.623
c_3	-0.087	-0.074
c_4	-0.732	-0.66
c_5	0.0978	0.121
c_6	-0.7	-0.53
c_7	-0.189	-0.159
c_8	-0.595	-0.57

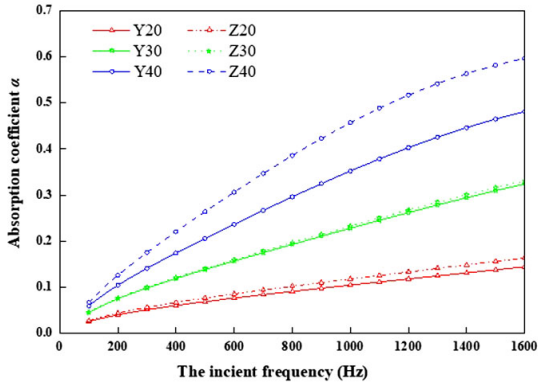

Fig. 6. The prediction curve of absorption characteristic using Garai-Pompoli model.

The Delany-Bazely model was put forward from measurements on fibers with a diameter between 1 and 10 μm, normally considered to be limited to the range $0.01 < \rho_0 f/r_0 < 1$. In contrast, the model Garai and Pompoli [35] proposed had a wider range of adaptability, available for the range $0.05 < \rho_0 f/r_0 < 8.4$. Both models have the same calculation structure but the coefficient are different, listed in Table 4.

When z_c and k_c are depended, the surface impedance z_s with a rigid backing can be calculated by

$$z_s = -jz_c \coth(k_c l) \tag{9}$$

where d was the depth of the fibrous materials.

The reflection coefficient is given by

$$R_c = \frac{z_s - \rho_0 c_0}{z_s + \rho_0 c_0}. \tag{10}$$

The absorption coefficient α can be obtained by Eq. (3). We calculated the adaptive parameters $\rho_0 f/r_0$ of six kinds of fibrous materials, and applied Garai-Pompoli model to predict absorption characteristic, shown in Fig. 6. Obviously, fibrous materials have obvious absorption effect on high-frequency sound waves, but little effect on low-frequency sound waves.

3.3 Acoustic absorption characteristic of porous sound absorber

The sound absorption characteristic curves of six kinds of fibrous material samples at different frequencies are displayed in Fig. 7. The incident sound frequency range is 105-465 Hz, the interlayer depth L_1 = 10 cm, the back cavity depth L_2 = 20 cm, and the airflow q_v = 9.5 m^3/h. The sound absorption curves of all samples show "barb type" in the whole frequency band, and the optimum sound absorption coefficient exceeded 0.95, proving the advantage of the porous sound absorber. According to the previous research results and theoretical prediction, the sound absorption performance of fibrous materials in low frequency band is poor [17] while the perforated plate has obvious advantages [38]. Combined fibrous materials with perforated plate, the sound absorption performance of porous sound absorber in low frequency band is strengthened. As we can see from Fig. 7(a), in a specific frequency range, the sound absorption effect of the sandwich structure is better with the gradual increase of the incident frequency, but the sound absorption effect begins to decrease significantly with the continuous growth of the incident frequency. It shows that there is an optimal sound absorption point for different samples. Compared with Figs. 7(a) and (b), the sound absorption coefficients of two kinds of fibrous materials are about 0.75 near 105 Hz, and then increase rapidly, when the growth of sound absorption effect of sandwich structure is most sensitive to the change of external sound excitation frequency. For coconut fiber samples, the sound absorption coefficient of Y30 is lower than Y40 in the lower frequency band, and its sound absorption curve gradually exceeds the latter with the increase of frequency. For palm bark fiber, the sound absorption curve of each sample in the low-frequency band is complex, and it shows more obvious regularity with the increase of frequency. In contrast with coconut fiber samples, it is evident that Z20, Z30 and Z40 have better sound absorption effects in the higher frequency band.

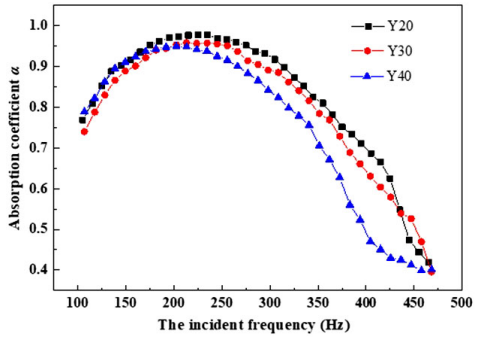

(a)

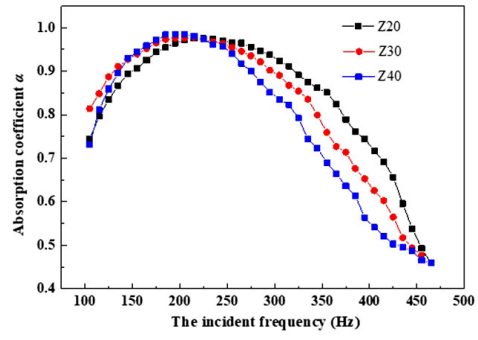

(b)

Fig. 7. Sound absorption coefficient at different frequencies experiments of two kinds of fibrous material: (a) coconut fiber; (b) palm bark fiber, in impedance tube, with L_1 = 10 cm, L_2 = 20 cm and $q_v = 2.64 \times 10^{-3}$ m^3/s.

The thickness of the sample is also an essential factor affecting sound absorption. The sound absorbers composed of samples with different thicknesses have their specificity. As illustrated in Fig. 7(a), the maximum sound absorption coefficient of the sandwich structure equipped with Y20 is 0.978 at 235 Hz, 0.971 at 205 Hz with Y30, and 0.963 at 195 Hz with Y40. It indicates that the optimal sound absorption frequency has a low-frequency offset with the increase of sample thickness, which is consistent with the sound absorption test results of Berardi et al. [19] and Mohammad et al. [22], using fibrous materials only. At the same time, the sample with large thickness has higher flow resistance, resulting in low sound absorption coefficient, which agreed with those reported by Bies [45] and Yilmaz [46]. The addition of a perforated plate has an imparity influence on the sound absorption effect during different frequencies, resulting in a lower sound absorption coefficient with thick samples in the high-frequency band. In the meanwhile, it is observed from the graph that in the higher frequency band, the sound absorption coefficients with two kinds of different thickness samples begin to show noticeable differences and return to their lowest points at about 465 Hz.

3.4 The effect of back cavity depth

It was reported that the fiber structure with air back cavity could strengthen the sound absorption performance of sound absorbers by previous studies [47]. In light of this, research on the influence of back cavity depth of fiber sandwich structure was essential. The interlayer depth between fibrous material and the perforated plate was fixed at L_1 = 10 cm. In the meanwhile, the incident sound wave frequency was set at f = 165 Hz and remains stationary. This frequency was selected on account of the main oscillating frequency of the ethanol flame burner near here, which could better restore the situation of the combustion process. By changing the number of back cavity cavities and adjusting the travel depth of the electric piston, the back cavity depth was controlled within the scope of L_2 = 100-400 mm. The variation of the sound absorption coefficient of sandwich structure as a function of back cavity depth is shown in Fig. 8.

It is obtained from the curve, increasing the depth of the back cavity can significantly improve the sound absorption effect of the sandwich structure because of the increase of the air gap thickness, which increases the impedance of the sound absorber and dissipates more sound energy [37]. The overall

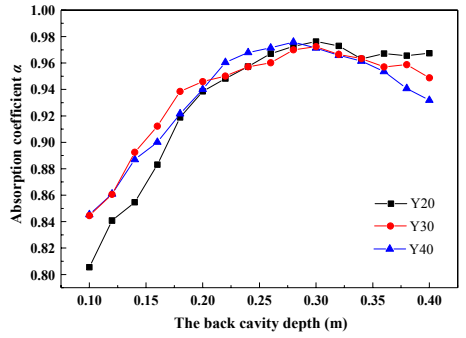

(a)

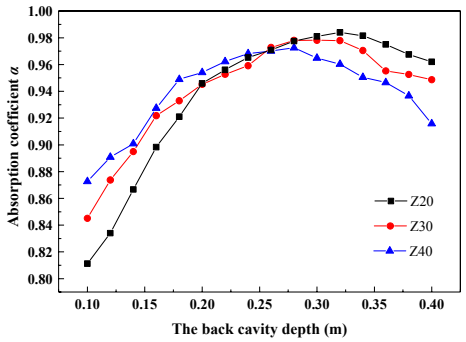

(b)

Fig. 8. Sound absorption coefficient of (a) coconut fiber; (b) palm bark fiber as a function of the back cavity depth in impedance tube, with f = 165 Hz, L_1 = 10 cm and q_v = 2.64×10^{-3} m^3/s.

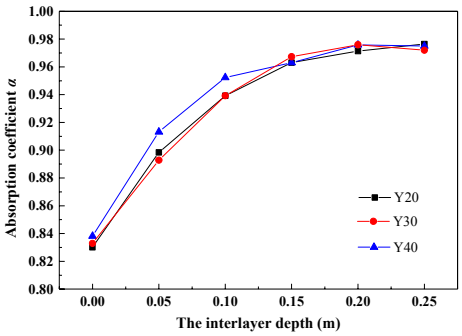

(a)

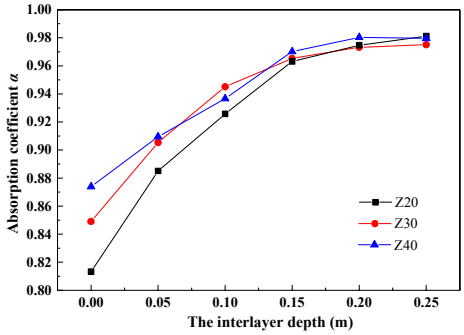

(b)

Fig. 9. Sound absorption coefficient of (a) coconut fiber; (b) palm bark fiber as a function of the interlayer cavity depth in impedance tube, with f = 165 Hz, L_1 = 10 cm and q_v = 2.64×10^{-3} m^3/s.

curve shows a trend of first increasing and then slightly decreasing, indicating an optimal cavity depth L_{op}, and the fiber sandwich structure works best when L_2 = L_{op}. The optimum cavity depth of the sandwich structure of each sample falls in the range of L_{op} = 280-320 mm, and the sound absorption coefficient is about α = 0.98. Interestingly, we found that the thicker the sample is, the better the sound absorption performance is in the low back cavity depth range within the test range. Additionally, with the increasing depth of the back cavity, the sound absorption coefficient of the thin sample increases faster than that of the thick sample, and the sound absorption coefficient finally exceeds that of the thick sample structure.

3.5 The effect of interlayer depth

According to the theory of acoustic electric analogy, the acoustic impedance of porous sound absorber is composed of fibrous material and perforated plate in series. The interlayer depth is an important factor of Helmholtz number He = kL_2 affecting the characteristic impedance of perforated plate in our previous study [12]. Therefore, the study of the influence of air layer depth between fibrous material and the perforated plate was also of significance. The depth of the back cavity was set at L_2 = 20 cm to maintain a single variable, and the sound absorption characteristic curve with the interlayer depth under the acoustic excitation of f = 165 Hz is displayed in Fig. 8. The sound absorption coefficient of the sandwich structure of each sample shows a gradual increasing trend with the increase of interlayer depth and remains unchanged after L_1 = 20 cm. This is because with the extension of interlayer depth, the Helmholtz number increases, increasing the sound resistance of porous sound absorber. As can be seen from Fig. 9(a), three curves of coconut fiber sample basically coincide, which proves that the change of sample thickness has little effect under different interlayer depths. As for the palm bark fiber sample, the thickness difference is shown when L_1 = 0, which reflects the law that the thicker the sample, the weaker the sound absorption capacity.

3.6 Control of combustion oscillations

This paper studied the control effect of fiber sandwich structure on ethanol flame combustion instability in a liquid-spray self-excited rig. The sandwich structures with Y30 and Z30 were selected for experimental research, due to moderate sound absorption characteristics. The fibrous material and perforated plate were installed at z = -L_1 and z = 0, respectively, which could play a role in heat insulation, shown in Fig. 5. The air sandwich depth and back cavity depth were set at the optimal depth L_1 = 20 cm and L_2 = 30 cm to determine the best control effect of the sandwich structure. Under the condition of no sandwich structure, the length of the inlet section only included the length of the 10 cm plenum chamber.

Fig. 10 shows the sound pressure level of oscillating ethanol

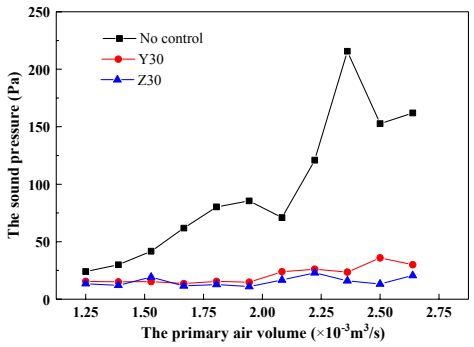

Fig. 10. The sound pressure as function of primary air flow rate before and after control in the combustion chamber, with L_1 = 20 cm and L_2 = 30 cm.

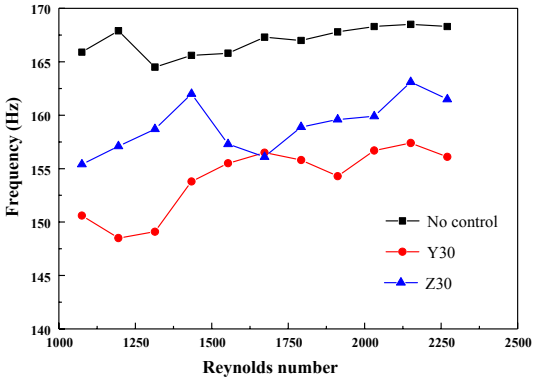

Fig. 11. Variation of sound frequency in the combustion chamber before and after control, with L_1 = 20 cm and L_2 = 30 cm.

flame in the combustion chamber before and after control under different primary airflow. The variation range of primary air volume is 1.25-2.64×10^{-3} m^3/s and the step size 0.14×10^{-3} m^3/s. It can be concluded that before control, the sound pressure in the combustion chamber gradually became stronger with the increase of primary airflow, and reached the maximum level of 216 Pa at 2.36×10^{-3} m^3/s, which indicates that the thermoacoustic oscillation intensity increased firstly and then declined with the decrease of equivalence ratio. When two kinds of porous sound absorber were adopted, the sound pressure level in the combustion chamber decreases obviously. The control effects of different fibrous materials were the same, for the reason that the fiber diameters of the two kinds of materials were similar and the sample thickness was the same, consistent with the acoustic test results of the impedance tube.

Fig. 11 is the variation diagram of the main oscillating frequency of ethanol flame oscillation in the combustion chamber before and after control. And the main oscillating frequency of the flame was reduced equipped with the porous sound absorber. It is well-known that the additional structure increases the inlet length of the combustion chamber, resulting in the deviation of the main frequency to the low frequency. Fig. 12 shows the sound pressure change in the plenum chamber. By contrast, the sound pressure in the plenum chamber was lower, although it also showed the same law as that in the combustion

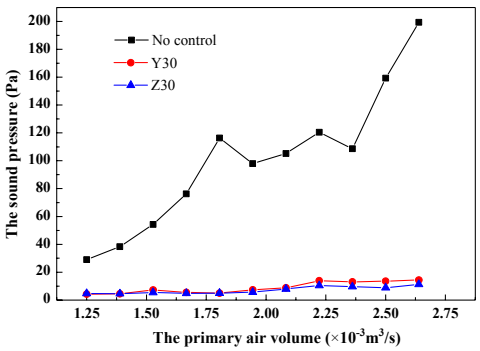

Fig. 12. The sound pressure as a function of primary airflow rate before and after control in the plenum chamber, with L_1 = 20 cm and L_2 = 30 cm.

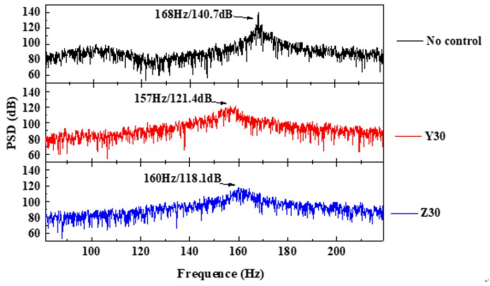

Fig. 13. PSD of the pressure in the combustion chamber before and after control, with L_1 = 20 cm and L_2 = 30 cm.

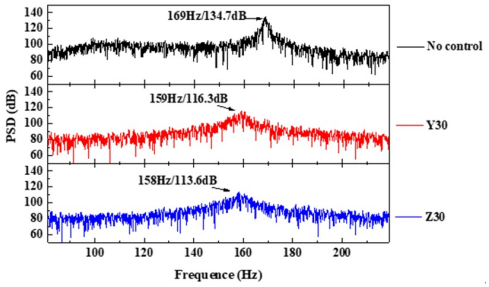

Fig. 14. PSD of the pressure in the plenum chamber before and after control, with L_1 = 20 cm and L_2 = 30 cm.

chamber.

The experiment was carried out under the combustion condition of Φ = 0.36 (primary air volume q_v = 2.36×10^{-3} /m^3/s and atomized air 10 L/min), the most apparent equivalence ratio for flame oscillation. The interlayer depth and back cavity depth were also set at L_1 = 20 cm and L_2 = 30 cm. The power spectral density (PSD) levels in the combustion chamber and plenum chamber were measured experimentally. It is concluded from Fig. 13 that main oscillating frequency without control was 168 Hz in the combustion chamber, which decreased to 157 Hz and 160 Hz after being controlled by the fiber sandwich structure due to the increase of the inlet length. What's more, the oscillation pressure decreased by 19.3 dB (89.2 %) and 22.6 dB (92.6 %), respectively. In contrast, the oscillation pressure in the plenum chamber is reduced by 18.4 dB (88.0 %) and 21.1 dB (91.2 %), seen in Fig. 14. It shows that the fiber

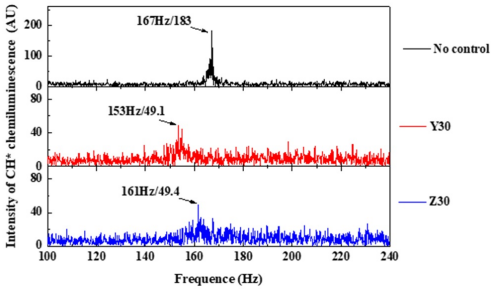

Fig. 15. Chemiluminescence intensity of CH* fluctuation in the combustion chamber before and after control, with L_1 = 20 cm and L_2 = 30 cm.

sandwich structure can control the oscillating ethanol flame, proving its effectiveness.

The structure controlling oscillating ethanol flame mechanism was explored by collecting the intensity of ethanol flame in the combustion chamber with photomultiplier tubes (PMT). The frequency and chemiluminescence intensity of the CH* fluctuation signal were drawn in Fig. 15. The fluctuation intensity of flame heat release was reduced by about 134 AU (73 %) compared with that before control, and the frequency was also reduced, which indicated that flame heat release was controlled.

In a word, the fiber sandwich structure can inhibit the sound source, as well as play the role of damping and dissipation in the propagation process, working together to realize the control of oscillating ethanol flame.

4. Conclusions

In this study, the sound absorption characteristics of fiber sandwich structure composed of coconut fiber, palm bark fiber and perforated plate were experimentally studied. The influences of various parameters of the structure on the sound absorption effect were measured in an impedance tube, as well as applied to the liquid-spray flame self-excited rig. The control effect of oscillating flame was also tested under hot conditions. The main conclusions are drawn as follows.

1) The fiber diameters of two kinds of fibrous materials were similar. The porous sound absorber with the same thickness fibrous materials had the similar sound absorption characteristics in 100-450 Hz. The sound absorption coefficient increased firstly and then decreased. And the maximum sound absorption coefficient exceeded 0.95.

2) Increasing the back cavity depth of porous sound absorber in a specific range could significantly improve its sound absorption coefficient. The optimal cavity depth of each sample appeared at about 30 cm, and the sound absorption coefficient was about 0.98.

3) With the increase of the interlayer depth between fibrous material and perforated plate, the sound absorption effect was enhanced. The sound absorption coefficient increased monotonically with the interlayer depth and tended to be flat at the optimal depth of about 20 cm.

4) The sound absorber with two kinds of fibrous materials could obviously suppress thermoacoustic instability. The oscillation pressure in the combustion chamber was reduced by 19.3 dB (89.2 %) and 22.6 dB (92.6 %), respectively, while 18.4 dB (88.0 %) and 21.1 dB (91.2 %) in the plenum chamber. The porous sound absorber could inhibit the sound source, as well as play the role of damping and dissipation in the propagation process, further consuming sound energy and strengthening sound absorption. Besides, the addition of the structure increases the inlet length of the burner, leading to a low-frequency offset on the main oscillating frequency of the flame.

Acknowledgments

This work was supported by the National Science Fund for Distinguished Young Scholars (No.51825605).

Nomenclature

General notations

m_0	: Mass of sample
l	: Thickness of sample
a	: Aperture radius
d	: Orifice spacing
h	: Plate thickness
x	: Location of impedance tube
f	: Incident frequency
s	: Sensor spacing
R_c	: Reflection coefficient
d_i	: Swirler diameter
d_o	: Swirling diameter
S_w	: Geometrical swirl number
z	: Location of self-excited burner
L_1	: Interlayer depth
L_2	: Back cavity depth
R	: Airflow resistance of the material
r_0	: Airflow resistivity of the material
Δp	: Differential pressure
A	: Cross-sectional area of the fibrous material
z_c	: Characteristic impedance
k_c	: Complex wave number of porous materials
c_0	: Sound velocity
z_s	: Surface impedance
q_v	: Primary air volume
L_{op}	: Optimum cavity depth
He	: Helmholtz number
k	: Complex wave number of cavity

Greek Letters

σ	: Plate porosity
ω	: Angle frequency
ζ	: Specific impedance
θ	: Phase of reflection coefficient

α : Absorption coefficient
ϕ : Global equivalence ratio
γ : Swirl angle
ρ_0 : Air density

Acronyms and abbreviations

SPL : Sound pressure level
PSD : Power spectral density

References

[1] A. P. Dowling, The challenges of lean premixed combustion, *Proceedings of the International Gas Turbine Congress* (2003).

[2] C. Tao and H. Zhou, Dilution effects of CO_2, Ar, N_2 and He microjets on the combustion dynamic and emission characteristics of unsteady premixed flame, *Aerospace Science and Technology*, 111 (2021) 106537.

[3] L. Li and D. Zhao, Prediction of stability behaviors of longitudinal and circumferential eigenmodes in a choked thermoacoustic combustor, *Aerospace Science and Technology*, 46 (10-11) (2015) 12-21.

[4] Y. Huang and V. Yang, Dynamics and stability of lean-premixed swirl-stabilized combustion, *Progress in Energy and Combustion Science*, 35 (4) (2009) 293-364.

[5] J. X. Li and A. S. Morgans, Simplified models for the thermodynamic properties along a combustor and their effect on thermoacoustic instability prediction, *Fuel*, 184 (15) (2016) 735-748.

[6] T. Lieuwen and V. Yang, Combustion instabilities in gas turbine engines: operational experience, fundamental mechanisms, and modeling, *Mechanical Engineering*, 128 (3) (2006) 44.

[7] Rayleigh, The explanation of certain acoustical phenomena, *Nature*, 18 (455) (1878) 319-321.

[8] S. Joo, S. Kwak, J. Lee and Y. Yoon, Thermoacoustic instability and flame transfer function in a lean direct injection model gas turbine combustor, *Aerospace Science and Technology*, 116 (2021) 106872.

[9] Z. G. Zhang et al., Transient energy growth of acoustic disturbances in triggering self-sustained thermoacoustic oscillations, *Energy*, 82 (15) (2015) 370-381.

[10] M. D. Garcia, E. Mastorakos and A. P. Dowling, Investigations on the self-excited oscillations in a kerosene spray flame, *Combustion and Flame*, 156 (2) (2009) 374-384.

[11] T. X. Yi and D. A. Santavicca, Combustion instability and flame structure of turbulent swirl-stabilized liquid-fueled combustion, *Journal of Propulsion and Power*, 28 (5) (2012) 1000-1014.

[12] H. Zhou et al., Attenuation effects of perforated plates with heterogeneously distributed holes on combustion instability in a spray flame combustor, *Journal of Mechanical Science and Technology*, 34 (11) (2020) 4865-4875.

[13] D. Chandramohan and K. Marimuthu, Applications of natural fiber composites for replacement of orthopaedic alloys, *International Conference on Nanoscience, Engineering and Technology (ICONSET 2011)* (2011) 137-145.

[14] B. I. Zabalza et al., Life cycle assessment of building materials: comparative analysis of energy and environmental impacts and evaluation of the eco-efficiency improvement potential, *Building and Environment*, 46 (5) (2011) 1133-1140.

[15] M. Davoodi et al., Effect of polybutylene terephthalate (PBT) on impact property improvement of hybrid kenaf/glass epoxy composite, *Materials Letters*, 67 (1) (2012) 5-7.

[16] M. Alhijazi et al., Recent developments in palm fibers composites: a review, *Journal of Polymers and the Environment*, 28 (2020) 3029-3054.

[17] U. Berardi and G. Iannace, Acoustic characterization of natural fibers for sound absorption applications, *Building and Environment*, 94 (2) (2015) 840-852.

[18] U Berardi, G. Iannace and M. Gabriele, The acoustic characterization of broom fibers, *Journal of Natural Fibers*, 14 (6) (2017) 858-863.

[19] N. H. Bhingare and S. Prakash, An experimental and theoretical investigation of coconut coir material for sound absorption characteristics, *Materials Today: Proceedings*, 43 (2) (2021) 1545-1551.

[20] A. Putra et al., Sound absorption of extracted pineapple-leaf fibres, *Applied Acoustics*, 136 (7) (2018) 9-15.

[21] M. Fouladi, M. Ayub and M. Nor, Analysis of coir fiber acoustical characteristics, *Applied Acoustics*, 72 (1) (2011) 35-42.

[22] K. O. Ballagh, Acoustical properties of wool, *Applied Acoustics*, 48 (2) (1996) 101-120.

[23] B. Bin et al., An experimental and simulation studies on sound absorption coefficients of banana fibers and their reinforced composites, *Nano Hybrids and Composites*, 12 (11) (2016) 9-20.

[24] S. Da et al., Sound absorption coefficient assessment of sisal, coconut husk and sugar cane fibers for low frequencies based on three different methods, *Applied Acoustics*, 156 (15) (2019) 92-100.

[25] K. Kalauni and S. J. Pawar, A review on the taxonomy, factors associated with sound absorption and theoretical modeling of porous sound absorbing materials, *Journal of Porous Materials*, 26 (6) (2019) 1795-1819.

[26] M. Hashim et al., The effect of alkali treatment under various conditions on physical properties of kenaf fiber, *Journal of Physics Conference Series*, 914 (2017) 012030.

[27] M. Alhijazi et al., Recent developments in luffa natural fiber composites: review, *Sustainability-Basel*, 12 (18) (2020) 1-25.

[28] P. Sabarinathan, K. Rajkumar and A. Gnanavelbabu, Investigation of mechanical properties of luffa cylindrical and flax reinforced hybrid polymer composite, *Journal of Advanced Engineering Research*, 3 (2) (2016) 124-127.

[29] K. Anbukarasi and S. Kalaiselvam, Study of effect of fibre volume and dimension on mechanical, thermal, a water absorption behaviour of luffa reinforced epoxy composites, *Materials and Design*, 66 (3) (2015) 321-330.

[30] V. Tanobe et al., Sponge gourd (luffa cylindrica) reinforced polyester composites: preparation and properties, *Defence Science Journal*, 64 (3) (2014) 273-280.

[31] I. Nasidi, L. Ismail and E. Samsudin, Effect of sodium hydrox-

ide (NaOH) treatment on coconut coir fibre and its effectiveness on enhancing sound absorption properties, *Pertanika Journal of Science and Technology*, 29 (1) (2021) 693-706.
[32] L. Cao et al., Porous materials for sound absorption, *Composites Communications*, 10 (2018) 25-35.
[33] M. Delany and E. Bazley, Acoustical properties of fibrous absorbent materials, *Applied Acoustics*, 48 (2) (1970) 105-116.
[34] D. Oldham, C. Egan and R. Cookson, Sustainable acoustic absorbers from the biomass, *Applied Acoustics*, 72 (6) (2011) 350-363.
[35] M. Garai and F. Pompoli, A simple empirical model of polyester fibre materials for acoustical applications, *Applied Acoustics*, 66 (12) (2005) 1383-1398.
[36] J. Allard and Y. Champoux, New empirical equations for sound-propagation in rigid frame fibrous materials, *Journal of the Acoustical Society of America*, 91 (6) (1992) 3346-3353.
[37] M. Fouladi et al., Enhancement of coir fiber normal incidence sound absorption coefficient, *Journal of Computational Acoustics*, 20 (1) (2012) 1250003.1-1250003.15.
[38] H. Zhou et al., Passive suppression of self-excited combustion instabilities in liquid spray flame using micro-perforated plate, *Journal of Engineering for Gas Turbines and Power*, 142 (11) (2020) 111013.
[39] ISO, ISO 10534-2:1998, *Acoustics − Determination of Sound Absorption Coefficient and Impedance in Impedance Tubes − Part 2: Transfer-Function Method* (1998).
[40] Y. Zhou, D. Zhao and T. Low, Experimental evaluation on acoustic impedance and sound absorption performances of porous foams with additives with Helmholtz number, *Aerospace Science and Technology*, 119 (2021) 107120.
[41] Y. Sun et al., Characterizing nonlinear dynamic features of self-sustained thermoacoustic oscillations in a premixed swirling combustor, *Applied Energy*, 264 (2020) 114698.
[42] N. Yilmaz et al., Effects of porosity, fiber size, and layering sequence on sound absorption performance of needle-punched nonwovens, *Journal of Applied Polymer Science*, 121 (5) (2011) 3056-3069.
[43] American Society for Testing and Materials, *ASTM C522: Standard Test Method for Airflow Resistance of Acoustical Materials* (2008).
[44] SIS, SS-EN 29053, *Acoustics - Materials for Acoustical Applications-Determination of Airflow Resistance*, Swedish Standard (1991).
[45] B. David and C. Hansen, *Engineering Noise Control: Theory and Practice*, Spon Press: New York (2003).
[46] N. D. Yilmaz et al., Effects of porosity, fiber size, and layering sequence on sound absorption performance of needle-punched nonwovens, *Journal of Applied Polymer Science*, 121 (5) (2011) 3056-3069.
[47] F. Lee and W. Chen, Acoustic transmission analysis of multilayer absorbers, *Journal of Sound and Vibration*, 248 (4) (2001) 621-634.

Hao Zhou is a Prof. at State Key Laboratory of Clean Energy Utilization, Zhejiang University, China. He received his Ph.D. in Zhejiang University. His research interests include combustion instability and gas turbine combustor design.

Hao Fang is a Ph.D. candidate in State Key Laboratory of Clean Energy Utilization, Zhejiang University, China. He received his B.S. degree from North China Electric Power University, China. His research interests include combustion instability and thermoacoustic.